Field-induced chaos in the Toda lattice

L. E. Reichl, R. de Fainchtein, T. Petrosky, and W. M. Zheng
Center for Studies in Statistical Mechanics, University of Texas, Austin, Texas 78712
(Received 7 September 1982)

When the two-particle periodic Toda lattice is perturbed by a time-dependent external field, we find that the external field creates resonance zones in the phase space of the Toda lattice. These resonance zones cause the energy of the lattice to undergo large fluctuations. Interaction of resonance zones causes the motion of the Toda lattice to become "chaotic." A theory is developed which describes the emergence of resonance zones for a small-amplitude applied field. Computer studies are presented which verify this theory.

I. INTRODUCTION

In recent years, there has been a resurgence of interest in the behavior of conservative anharmonic-oscillator systems. It was long thought that chaotic behavior in oscillator chains could be obtained simply by turning on a small anharmonicity. Early computer work by Fermi, Pasta, and Ulam[1] and by Henon and Heiles[2] showed that this was not true. The anharmonic systems studied by them remained coherent at low energies. The system studied by Henon and Heiles[2] only began to exhibit globally chaotic behavior above a certain critical energy. This is now fairly well understood in terms of work by Kolmogorov,[3] Arnol'd,[4] and Moser,[5] who showed theoretically that for large classes of anharmonic-oscillator systems the phase space was largely filled by invariant tori at low energy, thus ruling out globally chaotic behavior at low energy. The work of Chirikov,[6] Walker and Ford,[7] and others has shown that chaos in anharmonic-oscillator systems results from the interaction and overlap of resonance zones in phase space. These resonance zones have associated to them, wildly oscillating separatrices which allow trajectories to wander in an apparently random manner over large regions of the energy surface.

The work of Toda[8] illuminated another equally fascinating aspect of the behavior of anharmonic-oscillator systems. Toda found one particular anharmonic lattice that is completely integrable and could sustain propagation of coherent energy pulses (solitons). The solution of equations of motion of many-particle Toda lattices has been discussed by Flaschka,[9] and by Kac and Van Moerbeke.[10] The Toda lattice does not become chaotic at any energy. Computer simulation by Dancz and Rice[11] show that soliton propagation can also occur in nonintegrable anharmonic lattices, at least below the critical energy for onset of chaos where all coherent behavior is wiped out. Of great interest is the problem of how the small-scale chaos present in nonintegrable anharmonic systems affects soliton propagation.

As we shall show, an external field varying with time can be used to probe the effect of internal chaos on the propagation of nonlinear energy pulses (solitons). The problem of how an anharmonic system responds to external fields varying with time is important in other contexts as well. For example, the problem of how energy, absorbed from an external field, is distributed in a molecule and how the external field perturbs the internal dynamics of the molecule is not well understood. It is known that an external field varying with time can drive an otherwise well behaved nonlinear system into chaos. Yet, in few cases can the detailed mechanism be studied. As we shall show, the Toda lattice provides an ideal system for exploring the mechanism of field-induced chaos. In the absense of a field the N-particle Toda lattice is integrable. The solutions of the unperturbed system can be used to estimate where chaos will occur in the perturbed system. In this paper, we shall show how an external field drives the two-particle Toda lattice into chaos.

The two-particle Toda lattice reduces to a system of one degree of freedom after the center-of-mass motion has been removed. The methods we use in this paper can be used to describe the perturbation of any system of one degree of freedom. The Toda potential has the advantage that it is completely stable and has a very simple spectrum. Thus, it enables us to see clearly the interplay between the external field and the spectral properties of the unperturbed lattice.

We begin in Sec. II with a discussion of the properties of the unperturbed two-body Toda lattice, and we introduce a canonical transformation to a coordinate system in which one of the variables for the unperturbed lattice is cyclic. In Secs. III and IV we describe how an external field introduces resonance zones into the phase space of the perturbed system and give estimates for the size of chaotic regions. Comparison of the theory with numerical studies is given in Sec. V and, finally, in Sec. VI we make some concluding remarks.

II. UNPERTURBED TODA LATTICE

Let us consider a two-particle Toda lattice with cyclic boundary conditions (cf. Fig. 1). The Hamiltonian for this system can be written

$$H=\frac{P_1^2}{2m}+\frac{P_2^2}{2m}+\frac{A}{B}e^{B(Q_2-Q_1)}+\frac{A}{B}e^{B(Q_1-Q_2)}-\frac{2A}{B}\,, \tag{2.1}$$

where P_i and Q_i are the positions and coordinates, respectively, of the ith particle, m is the mass of the particles,

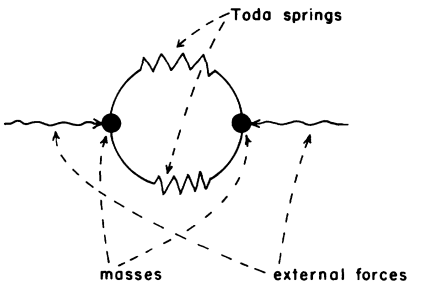

FIG. 1. Toda oscillator with applied field.

and A and B are constants which fix the scale of the potential.

It is convenient to make a canonical transformation to relative and center-of-mass coordinates. We let $P_{\text{c.m.}}=P_1+P_2$, $Q_{\text{c.m.}}=(Q_1+Q_2)/2$, $p=(P_1-P_2)/2$, and $q=(Q_1-Q_2)$. Then if we assume that $P_{\text{c.m.}}\equiv 0$, the Hamiltonian takes the form

$$H=\frac{p^2}{m}+\frac{A}{B}(e^{-qB}+e^{qB}-2)\ . \tag{2.2}$$

The equations of motion for this system are given by

$$\dot{p}=-\frac{\partial H}{\partial q}=A(e^{qB}-e^{-qB}) \tag{2.3a}$$

and

$$\dot{q}=\frac{\partial H}{\partial p}=\frac{2p}{m}\ . \tag{2.3b}$$

One can show without too much difficulty that the relative momentum $p(t)$ and relative position $q(t)$ evolve in time according to the equations

$$p(t)=\left[\frac{mA}{B}\right]^{1/2}\frac{2k}{(1-k^2)^{1/2}}\,\mathrm{sn}(\Phi,k) \tag{2.4}$$

and

$$q(t)=\frac{2}{B}\ln\left[\frac{\mathrm{dn}(\Phi,k)-k\,\mathrm{cn}(\Phi,k)}{(1-k^2)^{1/2}}\right], \tag{2.5}$$

where sn, dn, and cn are Jacobi elliptic functions, and

$$\Phi(t)=\frac{2Jt}{m_0}+\Phi_0\quad[\Phi_0=\Phi(0)]\ .$$

The modulus k is defined as

$$k^2=\frac{J^2-4m_0A/B}{J^2}\ . \tag{2.6}$$

In Eq. (2.6), $m_0=4m/B^2$ and J^2 is related to the total energy through the relation

$$H=\frac{J^2}{m_0}-\frac{4A}{B}\ . \tag{2.7}$$

The time series for $p(t)$ and $q(t)$ is periodic but is composed of an infinite number of Fourier components. This is easily seen if we note that

$$\mathrm{sn}(\Phi,k)=\frac{\pi}{Kk}\sum_{n=0}^{\infty}\frac{\sin[(2n+1)\Phi\pi/2K]}{\sinh[(2n+1)\Delta\pi/2]} \tag{2.8}$$

and

$$\ln[\mathrm{dn}(\Phi,k)-k\,\mathrm{cn}(\Phi,k)]=k\int^{\Phi}\mathrm{sn}(\Phi,k)d\Phi\ , \tag{2.9}$$

where $\Delta=K'/K$, and $K=K(k)$ and $K'=K(1-k^2)$ are complete elliptic integrals of the first kind. The spectrum of $p(t)$ and $q(t)$ will consist of odd multiples of the frequency $\Phi\pi/2K$. However, the amplitude associated with each frequency will decrease roughly exponentially with increasing n. It is easy to show that the variables (J,Φ) are canonical. Since $k\geq 0$, the canonical variable J can only take on values

$$|J|\geq 2\left[\frac{m_0A}{B}\right]^{1/2}\equiv J_{\min}\ . \tag{2.10}$$

Thus J can take on positive or negative values, however, condition (2.10) divides the (J,Φ) phase space into two disconnected parts. If we start with positive J we can never reach the region with negative J.

In Fig. 2, we show a plot of the (p,q) phase-space trajectory of the unperturbed Toda lattice for $A=0.15$, $B=3.1$, and $m=11.68\times 10^5$ in atomic units. (A and B were obtained by matching the Toda potential at low energy to that of the oxygen molecule. m is 40 times the mass of the oxygen atom.) The energy of the lattice is $E=0.302$ and $J=491$. For the above values of A, B, and m (the only

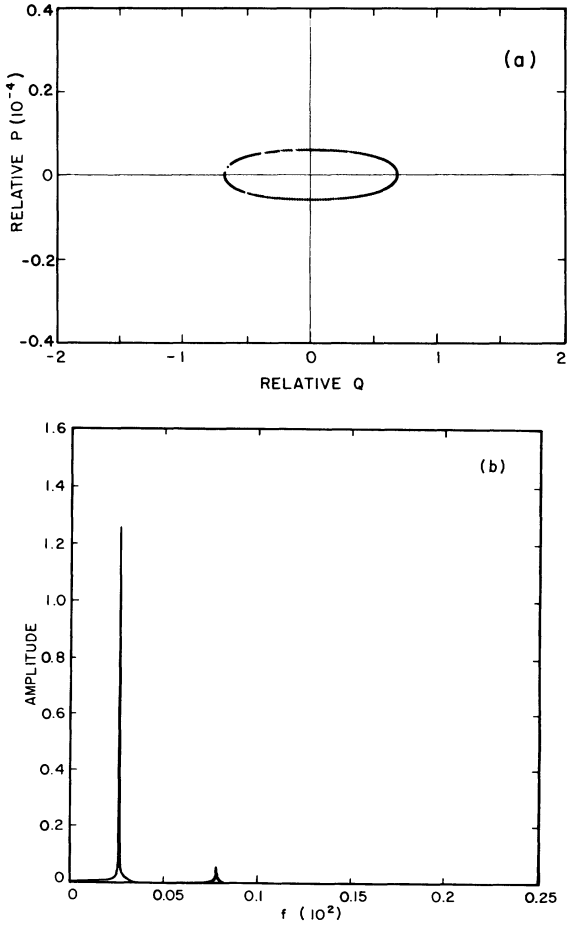

FIG. 2. (a) (p,q) phase-space trajectory and (b) spectrum of the unperturbed Toda lattice for $A=0.15$, $B=3.1$, and $m=11.68\times 10^5$.

ones we will consider in this paper) $J_{\min}=306$. In Fig. 2(b), we show the spectrum of the relative momentum at this same energy. We see that at this energy we are very near the harmonic limit of the oscillator, because most energy lies in a single-frequency mode of oscillation. A sketch of the (J,Φ) phase space is shown in Fig. 3. When the energy of the oscillator is constant, the (p,q) phase plot is an ellipse centered at the origin, and J is a straight line (J is constant).

We can now use these new canonical variables to obtain conditions under which an external field can induce large energy fluctuations and chaos in the Toda lattice.

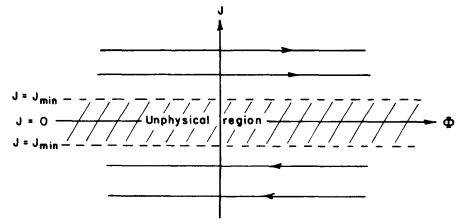

FIG. 3. Sketch of the unperturbed J,Φ phase space. Unphysical zone $-J_{\min}<J<J_{\min}$ divides the phase space into two disconnected parts. For $J>J_{\min}$ the phase trajectories (solid lines) all move in the direction of increasing Φ while for $J<J_{\min}$ they move in the direction of decreasing Φ.

III. PRIMARY RESONANCES IN THE PERTURBED TODA LATTICE

Let us apply an external force to each mass of the lattice in such a way that the center-of-mass momentum is zero (cf. Fig. 1). The Hamiltonian can be written

$$H=\frac{p^2}{m}+\frac{A}{B}(e^{-Bq}+e^{Bq}-2)+\epsilon q\cos\Omega_t\ , \tag{3.1}$$

where ϵ is the amplitude and $\Omega_t=\omega_0 t+\delta$ (ω_0 is the angular frequency, and δ is the phase of the applied field; in our strobe plots $\delta=\pi/2$). In terms of the canonical variables (J,Φ) the Hamiltonian becomes

$$H=\frac{J^2}{m_0}-4\frac{A}{B}+\frac{2\epsilon}{B}\cos\Omega_t\ln\left[\frac{\mathrm{dn}(\Phi,k)-k\,\mathrm{cn}(\Phi,k)}{1-k^2}\right]. \tag{3.2}$$

Then we can write the Hamiltonian in the form

$$H=\frac{J^2}{m_0}-\frac{4A}{B}+\epsilon\sum_{l=1,-1}\sum_{\substack{n=1\\(\mathrm{odd})}}^{\infty}g_n(J)\cos\left[\frac{n\Phi\pi}{2K(J)}-l\Omega_t\right]. \tag{3.3}$$

The sum over n involves only odd integers. The index l only takes values ±1. (Note that we have written K and Δ as functions of J rather than k to emphasize their dependence on J.) The function $g_n(J)$ may be obtained by the use of Eqs. (2.26) and (2.27). We find

$$g_n(J)=-\left[\frac{B}{2}n\sinh\left[n\frac{\pi K'}{2K}\right]\right]^{-1}. \tag{3.4}$$

The magnitude of $g_n(J)$ decreases roughly exponentially with increasing n.

The terms in Eq. (3.3) involving angle variations of the form

$$\cos\left[\frac{n\Phi\pi}{2K(J)}-l\Omega_t\right]$$

create resonance regions in the phase space for values of $J=J_n^c$ where

$$J_n^c=\frac{lm_0\omega_0}{n\pi}K(J_n^c)\ . \tag{3.5}$$

To see this let us focus on the region of the phase space near $J=J_n^c$ and let us make a time-dependent canonical transformation to a time-dependent coordinate system (P,ψ) and locate the zero value of P at $J=J_n\neq J_n^c$. This transformation can be accomplished by means of the time-dependent generating function

$$F(J,\psi,t)=-(J-J_n)(\psi+l\Omega_t)\frac{2K(J_n)}{n\pi}\ . \tag{3.6}$$

Then

$$P=-\frac{\partial F}{\partial\psi}=(J-J_n)\frac{2K(J_n)}{n\pi}\ , \tag{3.7}$$

$$\Phi=-\frac{\partial F}{\partial J}=(\psi+l\Omega_t)\frac{2K(J_n)}{n\pi}\ , \tag{3.8}$$

and the new Hamiltonian becomes

$$H'=H+\frac{\partial F}{\partial t}=\frac{\left[J_n+\dfrac{n\pi P}{2K(J_n)}\right]^2}{m_0}-\frac{4A}{B}-P\omega_0+\epsilon\sum_{l'}\sum_{\substack{n'=1\\(\mathrm{odd})}}^{\infty}g_{n'}\left[J_n+\frac{n\pi P}{2K(J_n)}\right]\cos\left[\frac{n'K(J_n)}{nK(J)}(\psi+l\Omega_t)-l'\Omega_t\right], \tag{3.9}$$

where n is odd.

Let us now restrict ourselves to very small values of P. Then we can write the Hamiltonian in the form

$$H'=\frac{J_n^2}{m_0}+\frac{n\pi PJ_n}{m_0K(J_n)}+\frac{n^2\pi^2P^2}{4m_0K^2(J_n)}-\frac{4A}{B}-P\omega_0+\epsilon\sum_{l}\sum_{\substack{n'\\(\mathrm{odd})}}g_{n'}(J_n)\cos\left[\frac{n'}{n}\psi+\left[\frac{n'l}{n}-l'\right]\Omega_t\right]+\cdots\ , \tag{3.10}$$

where we have neglected terms of higher order in the Taylor series. The equations of motion for P and ψ take the form

$$\dot{P}=-\frac{\partial H}{\partial \psi}=\epsilon\sum_{l}\sum_{n'}\frac{n'}{n}g_{n'}(J_n)\times\sin\left[\frac{n'}{n}\psi+\left[\frac{n'l}{n}-l\right]\Omega_t\right]+\cdots \tag{3.11}$$

and

$$\dot{\psi}=\frac{\partial H}{\partial P}=\frac{n\pi}{m_0K(J_n)}(J_n-J_n^c)+\frac{n^2\pi^2P}{2m_0K^2(J_n)}+\cdots . \tag{3.12}$$

From Eq. (3.11) we see that for small values of the product $\epsilon g_{n'}(J_n)$ changes in the value of P will be small. Neglecting the second term in Eq. (3.12), we see that for values of $J_n<J_n^c$ the direction of flow of $\psi(t)$ will be opposite to that of $\psi(t)$ for $J_n>J_n^c$. Thus the surface $J_n=J_n^c$ separates flow of opposite direction along the ψ direction, and we expect the region about $J_n=J_n^c$ to be strongly distorted.

The distortion of phase space at $J_n=J_n^c$ can also be viewed in another way. If we integrate the equations of motion then, for small $\epsilon g_n(J_n)$, we find

$$\psi(t)\simeq\frac{n\pi}{m_0K(J_n)}(J_n-J_n^c)t+\cdots \tag{3.13}$$

and

$$P(t)\simeq\frac{\epsilon g_n(J_n)\cos\psi(t)}{\frac{n\pi}{m_0K(J_n)}(J_n-J_n^c)}+\cdots . \tag{3.14}$$

Thus when $J_n\sim J_n^c$, the denominator in Eq. (3.14) goes to zero and $P(t)$ diverges indicating strong distortion of the phase space. This region of strong distortion is called the resonance zone.

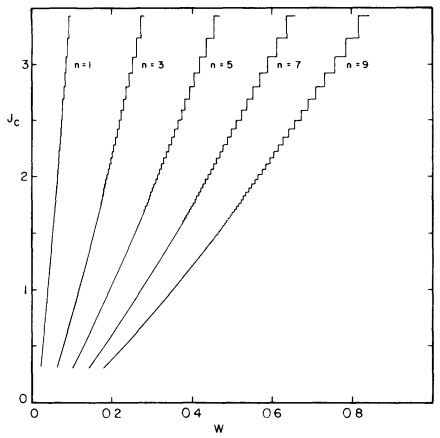

FIG. 4. Plot of J_n^c vs ω_0 for $n=1$, 3, 5, 7, and 9 for $A=0.15$, $B=3.1$, and $m=11.68\times10^5$.

The actual allowed values of J_n^c are found by solving Eq. (3.5) for J_n^c. This must be done numerically. Note that J_n^c is independent of ϵ but depends on ω_0 for small ϵ. The nth resonance zone first appears at $J=J_{\min}$ and at a frequency $\omega_0=\omega_{\min}^{(n)}$ where

$$\omega_{\min}^{(n)}=\frac{n\pi}{lm_0}\frac{J_{\min}}{K(J_{\min})} . \tag{3.15}$$

Thus the resonance zones appear at $J_{\min}$ in equally spaced frequency intervals. A plot of J_n^c versus ω_0 for $n=1$–9 is given in Fig. 4 for $A=0.15$, $B=3.1$, and $m=11.68\times10^5$.

Let us now study the flow about $J=J_n^c$. If we put $J_n=J_n^c$ in Eq. (3.10), we see that the term linear in P cancels and we find

$$H''=H'-\frac{J_n^2}{m_0}+\frac{4A}{B}=\frac{n^2\pi^2P^2}{4m_0K^2(J_n^c)}+\epsilon g_n(J_n^c)\cos(\psi)+\epsilon g_n(J_n^c)\cos(\psi+2\Omega_t)+\epsilon\sum_{l}\sum_{\substack{n',n\\ n'\neq n}}g_{n'}(J_n^c)\cos\left[\frac{n'}{n}\psi+\left[\frac{n'l}{n}-l'\right]\Omega_t\right] , \tag{3.16}$$

where we have introduced a new Hamiltonian H'' with a new zero point of energy.

In choosing $J_n=J_n^c$, we have focused on a strongly distorted region of the phase space, a resonance zone. To estimate the width of the resonance zone, let us neglect nonresonant interactions, i.e., the third and fourth terms in (3.16). The Hamiltonian is then approximated by

$$H''=\frac{P^2}{2I}+\epsilon g_n(J_n^c)\cos\psi , \tag{3.17}$$

where

$$I=\frac{2m_0K^2(J_n^c)}{n^2\pi^2} . \tag{3.18}$$

We will discuss this approximation below. The Hamiltonian (3.17) is just the Hamiltonian for a free pendulum with moment of inertia I. The angle ψ denotes angular displacement of the pendulum from its stable equilibrium position. The pendulum can undergo oscillations and rotation. As shown in Fig. 5, the line separating the two kinds of motion is called the separatrix. On the separatrix the motion must stop at its unstable equilibrium point, $\psi=\pi$. Thus the equation for the trajectory on the separatrix is given by

$$P_{sx}=\pm[2I\epsilon\,|\,g_n(J_n^c)\,|\,(1+\cos\psi_{sx})]^{1/2} . \tag{3.19}$$

From Eq. (3.19) the half-width of the resonance zone is

$$\Delta P_{sx}^{(n)}=2[I\epsilon\,|\,g_n(J_n^c)\,|\,]^{1/2} \tag{3.20}$$

or in terms of variable J [cf. (3.7)] it is

$$\Delta J_{sx}^{(n)}=[2m_0\epsilon\,|\,g_n(J_n^c)\,|\,]^{1/2} . \tag{3.21}$$

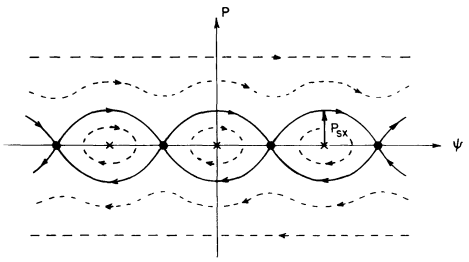

FIG. 5. Sketch of pendulum phase space. Solid line is the separatrix. Outside the separatrix we have rotation inside oscillation. Dark circles are unstable fixed points. Crosses are stable fixed points. Dotted and solid lines correspond to possible trajectories of the pendulum.

From this result, we see that the width of the resonance zones decreases roughly exponentially with increasing n. The width of all resonance zones increases with $\sqrt{\epsilon}$.

While the shape of the $n=1$ resonance zone will be described by the pendulum Hamiltonian, the separatrix associated with this zone will contain a stochastic layer induced primarily by the $n=1$ nonresonant interaction. The width of this stochastic layer may be estimated with the use of methods discussed by Chirikov.[6] Let us consider the first three terms in the Hamiltonian (3.16) and focus on $n=1$,

$$H''\simeq H_0-\epsilon\,|\,g_1(J_1^c)\,|\cos(\psi+2\Omega_t)\ , \tag{3.22}$$

where H_0 is the pendulum Hamiltonian

$$H_0=\frac{P^2}{2I}-\epsilon\,|\,g_1(J_1^c)\,|\cos\psi\ . \tag{3.23}$$

An orbit which lies on the separatrix of Hamiltonian H_0 has energy $H_0=E_0=\epsilon\,|\,g_1\,|\equiv I\omega^2$. The change in energy of an orbit on the separatrix (during one-half period of oscillation of the pendulum) due to the perturbation in Eq. (3.22) is given by

$$\begin{aligned}\Delta H_0&=\int_{-\infty}^{\infty}dt\frac{dH_0}{dt}\\&=\frac{-\epsilon\,|\,g_1\,|}{I}\int_{-\infty}^{\infty}dt\,P_{sx}(t)\sin[\psi_{sx}(t)+2\omega_0 t+\tau_0]\ ,\end{aligned} \tag{3.24}$$

where $P_{sx}(t)$ and $\psi_{sx}(t)$ describe the variation of momentum and angle at the separatrix. [We obtain explicit expressions for $P_{sx}(t)$ and $\psi_{sx}(t)$ by solving the equations of motion obtained from (3.23) for energy $H_0=\epsilon\,|\,g_1\,|$.] Equation (3.24) may be written in terms of Melnikov-Arnold integrals as described in Ref. 6. We find

$$\Delta H_0\simeq 32\pi I\omega_0^2 e^{-\pi\omega_0/\omega}\sin\tau_0\ . \tag{3.25}$$

Equation (3.25) may be used to set up the whisker map which describes motion in the neighborhood of the separatrix. The whisker map can then be used to obtain the half-width Δ_s of the stochastic layer at the separatrix. Δ_s is given by

$$\Delta_s=\frac{64\pi I\omega_0^3}{\omega}e^{-\pi\omega_0/\omega}\ . \tag{3.26}$$

We can use Eq. (3.26) to find the half-width of the stochastic layer in terms of the deviation δP from P_{sx}. We can write, in general,

$$I\omega^2+\Delta_s=\frac{P^2}{2I}-I\omega^2\cos\psi\ . \tag{3.27}$$

The angle $\psi=0$ locates the point on the separatrix where P_{sx} is largest, that is, $P_{sx}=\pm 2I\omega$. If we write $P=P_{sx}+\delta P$ and set $\psi=0$, we find

$$\Delta_s\simeq\frac{P_{sx}\delta P}{I}\ . \tag{3.28}$$

The angle $\psi=\pi$ locates the hyperbolic fixed point on the separatrix. There $P_{sx}=0$ and we find

$$\Delta_s\simeq\frac{(\delta P)^2}{2I}\ . \tag{3.29}$$

For later reference it is useful to compute δP for a particular example. Let us consider frequency $f_0=\omega_0/2\pi=5\times10^{-4}$. Then $J_1^c\simeq 1370$ and $\omega_0/\omega\simeq 3.5\epsilon$ [we have used $g_1(J_1^c)=0.665$ to obtain ω]. When $\epsilon=0.8$ and $\psi=0$ we have $P_{sx}=1334$ and $\delta P=20$. When $\epsilon=0.8$ and $\psi=\pi$ we have $P_{sx}=0$ and $\delta P=231$. Thus the stochastic layer near the hyperbolic fixed point is wider than elsewhere along the separatrix.

IV. SECONDARY RESONANCE ZONES (Ref. 12)

In Sec. III we derived conditions for the appearance of resonance zones in the phase space of the perturbed Toda lattice. However, we have not yet exhausted all possibilities. There are many more to be found. Additional resonance zones appear if we attempt to find the cyclic variables (J_1,Φ_1) associated with the full perturbed Hamiltonian (3.3). To see this, let us introduce the generating function

$$F_0(J_1,\Phi)=J_1\Phi+\epsilon G_0(J_1,\Phi,t)\ , \tag{4.1}$$

where

$$G_0(J_1,\Phi,t)=\sum_l\sum_{\substack{n\\(\text{odd})}}\frac{m_0 g_n(J_1)\sin[\kappa_n(J_1)\Phi-l\Omega_t]}{m_0\omega_0 l-2J_1\kappa_n(J_1)}\ , \tag{4.2}$$

where $\kappa_n(J_1)=n\pi/2K(J_1)$. The new canonical variables (J_1,Φ_1) are given in terms of the old variables (J,Φ_1), through the relations

$$\Phi_1=\frac{\partial F_0}{\partial J_1}=\Phi+\epsilon\frac{\partial G_0}{\partial J_1} \tag{4.3}$$

and

$$J=\frac{\partial F_0}{\partial\Phi}=J_1+\epsilon\frac{\partial G_0}{\partial\Phi}\ . \tag{4.4}$$

The transformed Hamiltonian H_1 is

$$H_1=\frac{J^2}{m_0}-\frac{4A}{B}+\epsilon V(J,\Phi)+\frac{\partial F_0}{\partial t}\ , \tag{4.5}$$

where

$$V(J,\Phi)=\sum_{l}\sum_{\substack{n\\(\text{odd})}} g_n(J)\cos[\kappa_n(J)\Phi-l\Omega_t]\ . \tag{4.6}$$

If we write H_1 explicitly in terms of the new canonical variables (J_1,Φ_1), by means of a Taylor-series expansion, we find

$$H_1=\frac{J_1^2}{m_0}+\epsilon^2\sum_{\substack{n_1,n_2\\(\text{odd})}}\sum_{l_1,l_2,l_3} g^{l_1,l_2}_{n_1,n_2}(J_1)\cos[\kappa^{l_3}_{n_1,n_2}(J_1)\Phi_1-L^{l_3}_{l_1,l_2}\Omega_t+\tau^{l_1,l_2}_{n_1,n_2}(J_1)]$$
$$+\epsilon^3\sum_{n_1,n_2,n_3}\sum_{l_1,l_2,l_3;l_1',l_2'} g^{l_1,l_2,l_3}_{n_1,n_2,n_3;l_1'}(J_1)\cos[\kappa^{l_1',l_2'}_{n_1,n_2,n_3}(J_1)\Phi_1-L^{l_1',l_2'}_{l_1,l_2,l_3}\Omega_t+\tau^{l_1,l_2,l_3}_{n_1,n_2,n_3;l_1'}]+O(\epsilon^4)\ , \tag{4.7}$$

where

$$\kappa^{l_3}_{n_1,n_2}(J_1)=\kappa_{n_1}(J_1)+l_3\kappa_{n_2}(J_1)\ , \tag{4.8a}$$

$$\kappa^{l_1',l_2'}_{n_1,n_2,n_3}=\kappa_{n_1}+l_1'\kappa_{n_2}+l_2'\kappa_{n_3}\ , \tag{4.8b}$$

$$L^{l_3}_{l_1,l_2}=l_1+l_2l_3\ , \tag{4.9a}$$

$$L^{l_1',l_2'}_{n_1,n_2,n_3}=l_1+l_1'l_2+l_2'l_3\ . \tag{4.9b}$$

The interaction $g^{l_1l_2}_{n_1n_2}(J_1)$ is given by

$$g^{l_1,l_2}_{n_1,n_2}(J_1)=\{[f^{l_1,l_2}_{n_1,n_2}(J_1)]^2+[h^{l_1,l_2}_{n_1,n_2}(J_1)]^2\}^{1/2}\ , \tag{4.10}$$

and the phase angle $\tau^{l_1,l_2}_{n_1,n_2}(J_1)$ is given by

$$\tau^{l_1,l_2}_{n_1,n_2}(J_1)=\tan^{-1}\left[\frac{h^{l_1,l_2}_{n_1,n_2}(J_1)}{f^{l_1,l_2}_{n_1,n_2}(J_1)}\right]\ . \tag{4.11}$$

In Eqs. (4.10) and (4.11),

$$f^{l_1,l_2}_{n_1,n_2}(J_1)=\frac{m_0}{2}\left[\frac{m_0g_{n_1}(J_1)g_{n_2}(J_1)\kappa_{n_1}(J_1)\kappa_{n_2}(J_1)}{[m_0\omega_0l_1-2J_1\kappa_{n_1}(J_1)][m_0\omega_0l_2-2J_1\kappa_{n_2}(J_1)]}+\frac{\dot g_{n_1}(J_1)g_{n_2}(J_1)\kappa_{n_2}(J_1)}{m_0\omega_0l_2-2J_1\kappa_{n_2}(J_1)}\right] \tag{4.12}$$

and

$$h^{l_1,l_2}_{n_1,n_2}(J_1)=\frac{m_0g_{n_1}(J_1)g_{n_2}(J_1)\dot\kappa_{n_1}(J_1)\kappa_{n_2}(J_1)}{2[m_0\omega_0l_2-2J_1\kappa_{n_2}(J_1)]}\ . \tag{4.13}$$

In Eqs. (4.12) and (4.13) we have used the notation $\dot g_n=dg_n/dJ$ and $\dot\kappa_n=d\kappa_n/dJ$. The interaction $g^{l_1,l_2,l_3}_{n_1,n_2,n_3;l_1'}(J)$ and phase angle $\tau^{l_1,l_2,l_3}_{n_1,n_2,n_3;l_1'}$ have a structure similar to $g^{l_1,l_2}_{n_1,n_2}$ and $\tau^{l_1'}_{n_1,n_2}$ but are more complicated. [For a special set of values of the indices $g^{l_1,l_2,l_3}_{n_1,n_2,n_3;l_1'}$ is given in Eq. (4.25).] The new canonical variables (J_1,Φ_1) are well defined as long as J_1 does not satisfy the odd-integer resonance condition given in Eq. (3.5) (To be more exact, as long as $\epsilon g_n(J_1)/[m_0\omega_0l-2J_1\kappa_n(J_1)]$ remains small.)

An analysis of the Hamiltonian H_1 similar to that given in Sec. III for the Hamiltonian H yields a new resonance condition on the variables J_1. We find

$$J_1^c=\frac{l_1+l_2l_3}{n_1+l_3n_2}\frac{m_0\omega_0K(J_1^c)}{\pi}\ . \tag{4.14}$$

Now instead of odd integer resonance zones we have the possibility of "fractional" or secondary resonance zones appearing. The width of these new zones is given by

$$\Delta J_{\rm sx}=[2m_0\epsilon^2\,|\,g^{l_1,l_2}_{n_1,n_2}(J_1^c)\,|\,]^{1/2}\ . \tag{4.15}$$

These new zones have a width proportional to ϵ rather than $\sqrt{\epsilon}$ as was the case for the odd-integer resonance zones introduced in Sec. III.

We can repeat this type of transformation. For example, we can transform to new canonical variables (J_2,Φ_2) via a generating function

$$F_1=J_2\Phi_1+\epsilon^2G_1(J_2,\Phi_1,t)\ , \tag{4.16a}$$

where

$$G_1(J_2,\Phi_1,t)=\sum_{\substack{n_1,n_2\\(\text{odd})}}\sum_{l_1,l_2,l_1'}\frac{m_0g^{l_1,l_2}_{n_1,n_2}(J)\sin[\kappa^{l_1'}_{n_1,n_2}(J_2)\Phi_1-L^{l_1'}_{l_1,l_2}\Omega_t+\tau^{l_1'}_{n_1,n_2}]}{m_0L^{l_1'}_{l_1,l_2}\omega_0-2J_2\kappa^{l_1'}_{n_1,n_2}(J_2)}\ . \tag{4.16b}$$

With this transformation we remove the contribution of order ϵ^2 in Eq. (4.7) and we are left with a leading contribution of order ϵ^3. This gives a new Hamiltonian,

$$H_2=\frac{J_2^2}{m_0}-\frac{4A}{B}+\epsilon^3\sum_{\substack{n_1,n_2,n_3\\(\text{odd})}}\sum_{l_1,l_2,l_3}\sum_{l_1',l_2'} g^{l_1,l_2,l_3}_{n_1,n_2,n_3;l_1'}(J_2)\cos[\kappa^{l_1',l_2'}_{n_1,n_2,n_3}(J_2)\Phi_2-L^{l_1',l_2'}_{l_1,l_2,l_3}\Omega_t+\tau^{l_1,l_2,l_3}_{n_1,n_2,n_3;l_1'}]+O(\epsilon^4)\ . \tag{4.17}$$

The new canonical variables (J_2,Φ_2) are well defined as long as we avoid resonance zones given by Eqs. (3.5) and (4.14). Analysis of the Hamiltonian (4.17) yields a new resonance condition

$$J_2^c=\frac{l_1+l_1'l_2+l_2'l_3}{n_1+l_1'n_2+l_2'n_3}\frac{m_0\omega_0K(J_2^c)}{\pi} . \tag{4.18}$$

The width of these new zones is given by

$$\Delta J_2^{\rm sx}=[2m_0\epsilon^3\,|\,g^{l_1,l_2,l_3}_{n_1,n_2,n_3;l_1'}(J_2^c)\,|\,]^{1/2} . \tag{4.19}$$

We may continue this type of transformation to eliminate terms of higher order[13] in ϵ. Each new set of canonical variables (J_i,Φ_i) introduces new resonance conditions. Indeed, resonance zones introduced will be dense in the phase space. It is useful to introduce a general resonance condition

$$J^c=\frac{M_0\omega_0K(J^c)}{\eta\pi} . \tag{4.20}$$

η can now take on all rational fractional values.

The resonance zones located by Eq. (4.20) are observable. The canonical transformations (4.2), and (4.16), etc. provide a means of solving the equations of motion of the system to any order in ϵ. To see this, let us stop after the second transformation and approximate the Hamiltonian H_2 by

$$H_2\simeq\frac{J_2^2}{m_0}-\frac{4A}{B} . \tag{4.21}$$

Then $J_2=$const and $\Phi_2=(2J_2/m_0)t+\delta_2$. The variables J_2 and Φ_1 may be expressed

$$J_1=J_2+\epsilon^2\frac{\partial G_{(1)}(J_2,\Phi_1,t)}{\partial\Phi_1} \tag{4.22}$$

and

$$\begin{aligned}\Phi_1&=\Phi_2-\epsilon^2\frac{\partial G_{(1)}}{\partial J_2}(J_2,\Phi_1,t)\\&=\frac{\partial J_2t}{m_0}+\delta_2-\epsilon^2\frac{\partial G_{(1)}}{\partial J_2}(J_2,\Phi_1,t) .\end{aligned} \tag{4.23}$$

We can, in principle, solve Eq. (4.23) for J_1 in terms of J_2 and t. Thus

$$\Phi_1=f(\epsilon,J_2,t) , \tag{4.24}$$

where $f(\epsilon,J_2,t)$ is some function of ϵ, J_2, and t. If we now combine Eqs. (4.4), (4.22), and (4.24) we see that J will contain resonance denominators which go to zero when condition (4.14) is satisfied. These denominators occur in terms of order ϵ^2. Resonance denominators which go to zero when Eq. (4.18) is satisfied first appear in terms of order ϵ^3 in the perturbation expansion of J.

Let us now locate some of these new resonance zones. The resonance condition (4.14) does not allow resonance zones to appear below $f_0=2.0\times10^{-4}$ as was the case with condition (3.5). However, it does allow even integer zones above $f_0=2.0\times10^{-4}$. The zone with the largest width will occur for $n_1=3$, $n_2=1$, $l_1=1$, and $l_2=l_1'=-1$; that is, $\eta=2$ [cf. Eqs. (4.14) and (4.20)]. It will first appear at frequency $f_0\pm4.0\times10^{-4}$. From Eq. (4.15) we find that it will have a width small compared to that of zone $\eta=1$ as long as ϵ is small. When $\epsilon=1$ it can become comparable in size to zone $\eta=1$. To see this, let us locate and compute the widths of these two zones for $f_0=5.0\times10^{-4}$. From Eqs. (3.5) and (3.21), we find that zone $\eta=1$ is located at $J^c=1370$ in J space with a half-width $\Delta J^{\rm sx}=804\epsilon$. From Eqs. (4.14) and (4.15) we find that the zone $\eta=2$ is located at $J_1^c=462$ in J_1 space and $\Delta J_1^{\rm sx}=67\epsilon$. It is easy to see that higher-order even-integer resonance zones will decrease rapidly in width because of the exponential decrease of g_n. As in Sec. IV, we can compute the width of the stochastic layer associated with zone $\eta=2$ due to nonresonant perturbations, but it is completely negligible ($\delta P\sim10^{-13}P_{\rm sx}$ when $\epsilon=1$).

Resonance condition (4.18) predicts that a resonance zone will occur for $\eta=\frac{1}{3}$ as well as for values of $\eta>1$. The zone $\eta=\frac{1}{3}$ will first appear at $f_0=\pm0.7\times10^{-4}$ and should become fairly important when $\epsilon\sim1$. The zone $\eta=\frac{1}{3}$ occurs for certain combinations of n_i and l_i. The leading terms are given by $n_1=n_2=n_3=1$, $l_1=l_2=l_1'=1$, and $l_3=l_2=-1$; and $n_1=3$, $n_2=n_3=1$, $l_1=1$, and $l_2=l_3=l_1'=l_2'=-1$. The effective interaction *for these two special cases* can be written

$$\begin{aligned}g^{l_1,l_2,l_3}_{n_1,n_2,n_3;l_1'}&=\frac{m_0^2g_{n_2}g_{n_3}\kappa_{n_2}\kappa_{n_3}}{8(m_0\omega_0l_2-2J^c\kappa_{n_2})(m_0\omega_0l_3-2J^c\kappa_{n_3})}\\&\times\{[\ddot g_{n_1}-g_{n_1}\dot\kappa_{n_1}(\dot\kappa_{n_1})^2]^2\\&\quad+[2\dot g_{n_1}\dot\kappa_{n_1}+g_{n_1}(\dot\kappa_{n_1})^2]^2\}^{1/2} .\end{aligned} \tag{4.25}$$

It is useful to locate and compute the width of the zone $\eta=\frac{1}{3}$ for $f_0=1.0\times10^{-4}$. We find $J_2^c=639$ in J_2 space and $\Delta J_2^{\rm sx}\sim63\epsilon^{3/2}$. Thus, for $\epsilon\sim1$, this zone can have significant effect on the motion of the Toda lattice.

Higher-order resonance conditions will allow more resonance zones to form for $f_0\le2.0\times10^{-4}$. However, they should become less important, at least for $\epsilon\le1$. The main reason is that the identity $\kappa_{nn}^{-1}(J)\equiv0$ prohibits any higher-order interaction from depending only on products of g_1. It must always contain many factors of g_n for $n>1$ or derivatives of g_n, both of which are small, and decrease exponentially with increasing n.

V. NUMERICAL RESULTS

Let us now consider numerical evidence of the resonance zones described in Secs. III and IV. In Fig. 6, we give a phase diagram of chaotic regions of the (p,q) phase space obtained from strobe plots of the (p,q) phase space. The phase plot shows regions of "chaos" as a function of frequency and amplitude of the applied field. To obtain this phase diagram we always started with the oscillator at an energy $E=0.302$ or $J_0=491$, and then by solving the equations of motion for the perturbed system we plotted p versus q at time intervals $1/f_0$. Figure 6 shows values of ϵ and f_0 for which the strobe plots appeared to contain chaos. We have distinguished between points of obvious chaos (the crosses), points of marginal chaos (the triangles), and points of no chaos (the dots). Points which con-

tain neither crosses, triangles, nor points have not been explored. We have found that the theory developed in previous sections gives us a good qualitative idea of where the resonances lie, at least for small $\epsilon g_n(J_n^c)$.

Let us examine some of the strobe plots which gave rise to the phase diagram in Fig. 6. We note that the resonance zone $\eta=1$ should emerge at $J^c_{\eta=1}=306$ at a frequency of $f_0=2.0\times10^{-4}$ (cf. Fig. 4) and for ϵ small it should give the strongest perturbation in the phase space. As we increase the frequency it moves to larger values of $J^c_{\eta=1}$. We are observing the phase space at $J=491$. Thus we do not expect to observe the first resonance until a frequency $f_0>2\times10^{-4}$. As ϵ increases, it will widen and we expect to see evidence of it at lower frequency the larger ϵ is.

Let us now examine the strobe plots. At $\epsilon=0.01$ we do not see evidence of the first resonance zone at $f_0=2\times10^{-4}$ or $f_0=3\times10^{-4}$. However, we do see it at $\epsilon=0.1$. In Fig. 7, we give the strobe plots for $\epsilon=0.1$ and $f_0=1\times10^{-4}$, 2×10^{-4}, 3×10^{-4}, and 4×10^{-4}. At $f_0=1\times10^{-4}$ [Fig. 7(a)] we see no evidence of the resonance zone. The strobe plot is an ellipse centered at the origin, indicating that $J=$const and the energy of the oscillator is roughly constant (see the discussion at the end of Sec. II). At $f_0=2\times10^{-4}$ [Fig. 7(b)] we see the resonance zone passing through. The ellipse is distorted and displaced. The value of J for the oscillator varies between $J\simeq327$ and 493, so the top of the resonance zone has entered the region we are exploring (see Fig. 5). At $f_0=3\times10^{-4}$ [Fig. 7(c)] we are inside the resonance zone. J now varies between $J\simeq493$ and 800, and the oscillator experiences large regular variations in energy. Finally, at $f_0=4\times10^{-4}$ [Fig. 7(d)] the resonance zone $\eta=1$ has passed through but is still influencing, slightly, the phase space. Thus, for small ϵ the theory does predict correctly the frequency of emergence of the resonance zones.

Let us next examine the strobe plots at $f_0=5\times10^{-4}$ for field amplitudes $\epsilon=0.01$, 0.1, 0.5, 0.7, and 0.8 [cf. Figs. 8(a)–8(e)]. At $\epsilon=0.01$, the system remains at constant energy. There appears to be no resonance zone nearby to affect its behavior. When $\epsilon=0.1$ the system trajectory is pulled to higher energies. This is due to zone $n=1$ which lies at higher energy but is beginning to broaden and affect

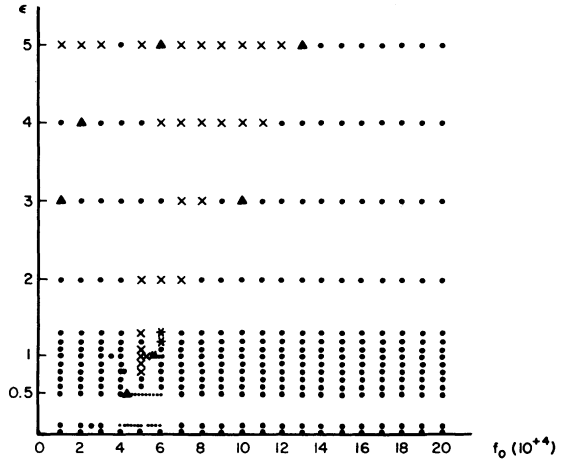

FIG. 6. Phase diagram of regions of field-induced chaos (as a function of amplitude ϵ, and frequency ω_0, of the applied field). Crosses show regions of obvious chaos. Triangles show regions of marginal chaos. Stars show regions for which chaos lies between marginal and obvious. Dots show regions with no chaos. No strobe plots were obtained for unmarked regions.

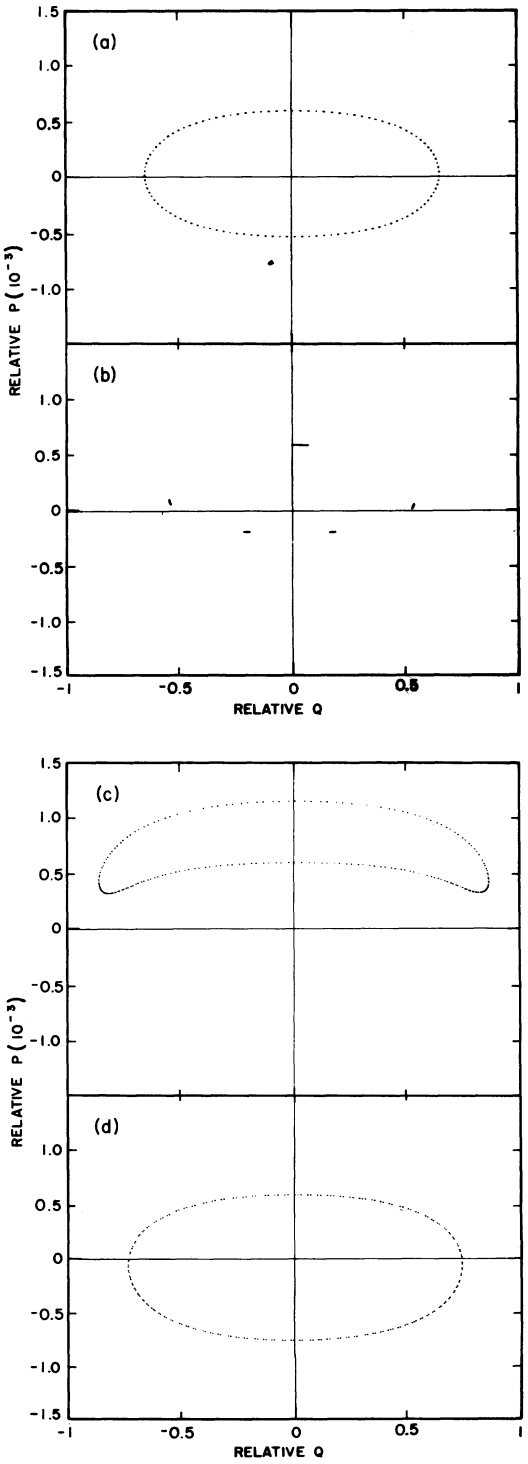

FIG. 7. Passage of the first resonance zone at $\epsilon=0.1$ as frequency is varied; (a) $f_0=1\times10^{-4}$, (b) $f_0=2\times10^{-4}$, (c) $f_0=3\times10^{-4}$, (d) $f_0=4\times10^{-4}$.

the region at $J=490$. As ϵ increases this effect becomes stronger until at $\epsilon=0.8$ the $n=1$ resonance zone actually enters the region of phase space which we are exploring [cf. Fig. 8(e)]. Here we see the shape of the separatrix for $n=1$ resonance zone. It is useful to introduce a quantity $\mathscr{H}$ which we define [see Eq. (3.9)] as

$$\mathscr{H}\simeq\frac{J^2}{m_0}-4\frac{A}{B}+\epsilon g_1\cos(\kappa_1\Phi-\omega_0 t-\pi/2)-\frac{\omega_0 J}{\kappa_1}\,, \tag{5.1}$$

where $\kappa_1=\pi/2K$. If we neglect variations of g_1 and κ_1 with J (these are in fact small), $\mathscr{H}$ is a constant of the motion, $d\mathscr{H}/dt\equiv 0$, and is sometimes called the quasienergy. At frequency $f_0=5\times10^{-4}$ the resonance zone $n=1$ is located at $J_1^c=1370$. For this value of J_1^c, $\kappa_1=0.54$ and $g_1=0.665$. In the strobe plot (Fig. 8) we are plotting the relative momentum

$$p=\frac{B}{2}(J^2-4m_0\mu)^{1/2}\mathrm{sn}(\Phi,k)\,,$$

and relative position

$$q=\frac{2}{B}\ln\left[\frac{\mathrm{dn}(\Phi,k)-k\,\mathrm{cn}(\Phi,k)}{(1-k^2)^{1/2}}\right],$$

at times $t=2N\pi/\omega_0$ where $N=(0,1,2,\ldots)$. Thus the quasienergy is always given by

$$\mathscr{H}=\frac{J^2}{m_0}-4\frac{A}{B}+\epsilon g_1\cos\left[\kappa_1\Phi-\frac{\pi}{2}\right]-\frac{\omega_0 J}{\kappa_1} \tag{5.2}$$

for the strobe plot in Fig. 8(e) and is approximately a constant of the motion. The allowed values of J and Φ are constrained by Eq. (5.2). That is why we see rather well-

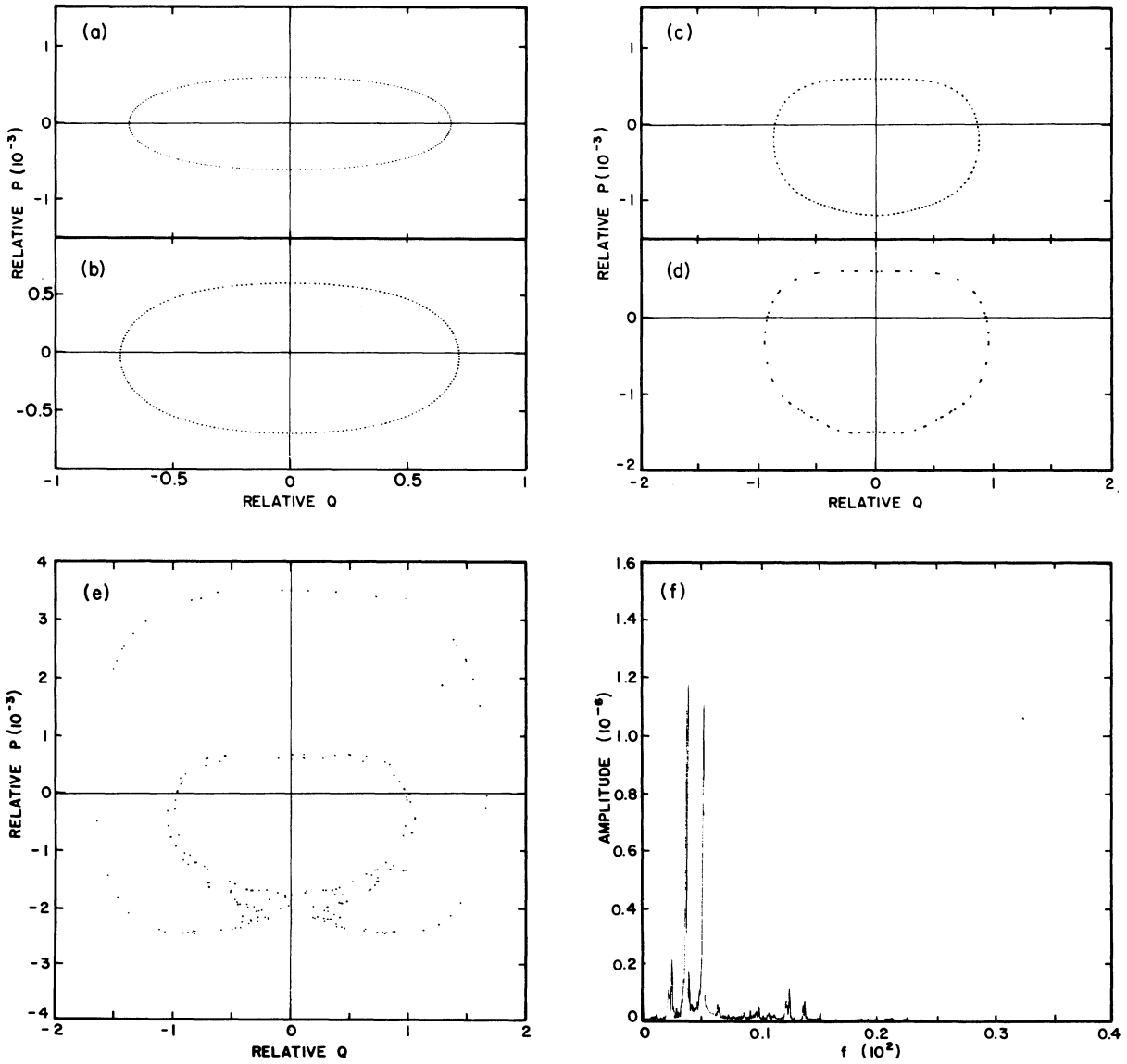

FIG. 8. A sequence of strobe plots showing the emergence of resonance zones at $f_0=5\times10^{-4}$ as ϵ increases; (a) $\epsilon=0.01$, (b) $\epsilon=0.1$, (c) $\epsilon=0.5$, (d) $\epsilon=0.7$, (e) $\epsilon=0.8$, (f) spectrum of relative momentum time series for $\epsilon=0.8$ and $f_0=5\times10^{-4}$.

defined curves in the strobe plots. Let us now write Eq. (5.2) in the form

$$\frac{(J-J_1^c)^2}{m_0}-\epsilon|g_1|\cos\left[\kappa_1\Phi-\frac{\pi}{2}\right]=\epsilon|g_1| \ . \tag{5.3}$$

If we choose $|g_1|=1.04$, Eq. (5.3) reproduces the curve in Fig. 9(e) to a very good approximation. The fact that we must use an experimental value of g_1 rather than its value for $J=J_1^c$ is reasonable since in Eq. (5.2) the value of g_1 varies over the range of values of J traced out by the curve in Fig. 8(e). The hyperbolic fixed point in Fig. 9(e) (located at $p=-592$ and $q=0$) occurs for $\Phi=K$. We see that there is a relatively broad stochastic layer surrounding this point. The width of this layer can be estimated from Eq. (5.34). We find that Δp, the half-width of the stochastic layer at the hyperbolic fixed point, is $\Delta p=198$. Note that Δp denotes the width of the stochastic region of the momentum of the Toda oscillator. This is in good agreement with what we observe in Fig. 8(e).

In Fig. 8(f) we give the spectrum of the time series for the relative momentum of the oscillator at $\epsilon=0.8$ and $f_0=5\times10^{-4}$. Here we see that the spectrum, while dominated by a few well-defined spectral lines, has begun to broaden. Thus the motion of the oscillator is still predominantly quasiperiodic but it also contains small-scale chaos as is evident in the strobe plot [Fig. 8(e)]. It is interesting to show the strobe plot and spectrum for $\epsilon=5.0$ and $f_0=9\times10^{-4}$ (see Fig. 9). Here the strobe plot indicates chaotic behavior on a larger scale and the markedly broadened spectrum reflects this fact.

The most dramatic evidence for the existence of the secondary resonance zones can be found by examining strobe plots of the Toda lattice at frequency $f_0=1\times10^{-4}$, where no odd-integer resonance zones exist. In Fig. 10, we give a sequence of strobe plots for frequency $f=1\times10^{-4}$ and $\epsilon=0.01$, 0.5, 0.7, 0.9, 1.1, 1.3, 2.0, 3.0, 4.0, 5.0, and 10.0 [the case $\epsilon=0.1$ is given in Fig. 7(a)]. We see that for $\epsilon=0.01$ and 0.1 [Figs. 10(a) and 7(a)] there is no resonance zone evident in the strobe plots. However, at $\epsilon=0.5$ [Fig. 10(b)] a resonance zone is approaching from below. At $\epsilon=0.7$ [Fig. 10(c)] we appear to be inside a resonance zone. At $\epsilon=0.9$ [Fig. 10(d)] we appear to be at the center of a higher-order resonance zone. At $\epsilon=1.1$, 1.2, and 1.3 [Figs. 10(e)–10(g)] the higher-order resonance zone is becoming wider as ϵ increases or we may be seeing a sequence of zones going past. At $\epsilon=3.0$ [Fig. 10(h)] we find a narrow instability zone with small-scale random fluctuations. At $\epsilon=4.0$ [Fig. 10(i)] we are at the center of a new resonance zone and at $\epsilon=5.0$ and 10.0 [Figs. 10(j) and 10(k)] the phase space is chaotic with large-scale fluctuations in the energy of the oscillator.

The appearance of resonance zones as ϵ is varied, holding f_0 fixed, is consistent with the theory of secondary resonances. The strobe plots show the behavior of the Toda oscillator in terms of physical variables (p,q) or (via an ϵ-independent transformation) the variables (J,Φ). The secondary resonance zones are located in (J_i,Φ_i) space which is related to (J,Φ) via an ϵ-dependent canonical transformation. Thus not only do we expect to see resonance effects for $f_0=1.0\times10^{-4}$ due to secondary resonance zones but also when viewed in (p,q) space we expect to see them change as ϵ is changed.

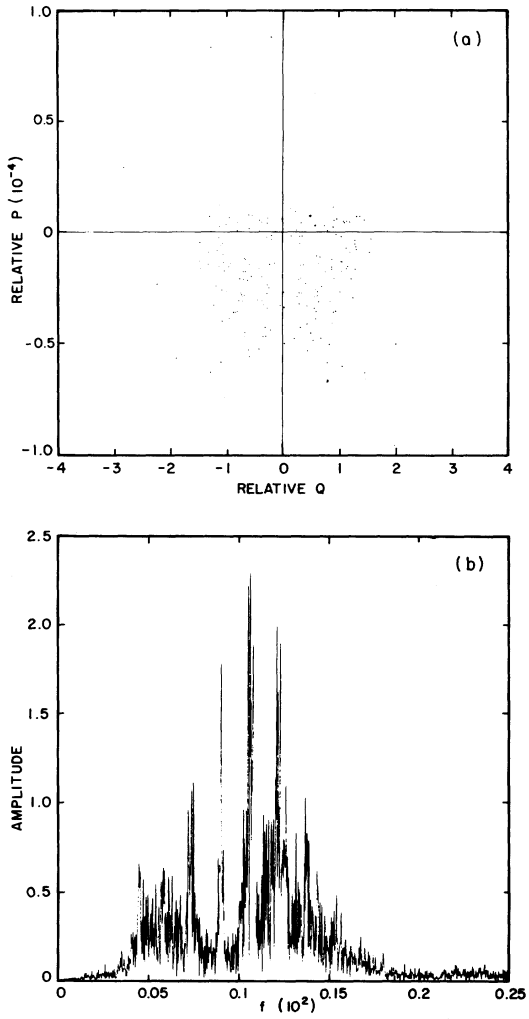

FIG. 9. (a) strobe plot at $\epsilon=5.0$ and $f_0=9\times10^{-4}$; (b) the spectrum of the relative momentum of the oscillator at this amplitude and frequency.

Let us now focus on Fig. 10(c). This plot appears to be an $\eta=\frac{1}{3}$ resonance zone. The quasienergy associated with this zone is

$$\mathcal{H}=\frac{J^2}{m_0}-V\cos\left[\kappa\Phi-3\omega_0 t-\frac{\pi}{2}\right]-\frac{\omega_0}{\kappa}J \ , \tag{5.4}$$

where V is an effective interaction. For $f_0=1\times10^{-4}$, $J_2^c=640$. For small ϵ, $J_2^c\sim J^c$. The relative momentum corresponding to this critical value is $p_c=870$. This value lies within the figure in the strobe plot. The trajectory in the strobe plot lies inside the separatrix for the $\eta=\frac{1}{3}$ resonance zone. The separatrix itself will have a shape similar to that in Fig. 8(e). Its hyperbolic fixed point will be at about $p=870$ and $q=0$.

VI. CONCLUDING REMARKS

Our purpose in studying the effect of a dynamic external field on the two-particle Toda lattice was to show the mechanism by which a dynamic field can disrupt even the simplest, most stable, nonlinear system. In the presence of

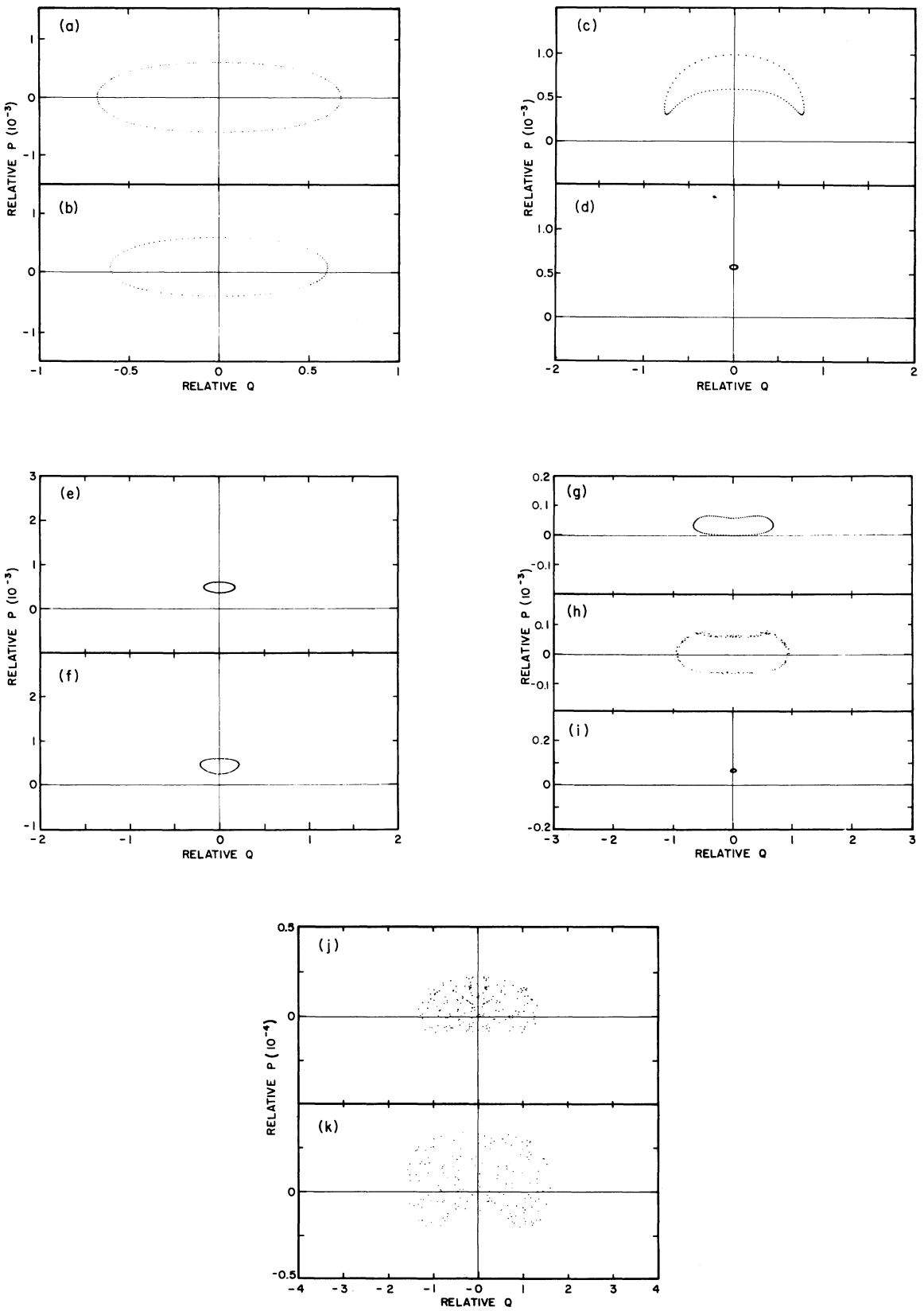

FIG. 10. A sequence of strobe plots showing the emergence of resonance zones when the frequency of the applied field is held fixed at $f_0 = 1 \times 10^{-4}$, but its amplitude is increased: (a) $\epsilon = 0.01$, (b) $\epsilon = 0.5$, (c) $\epsilon = 0.7$, (d) $\epsilon = 0.9$, (e) $\epsilon = 1.1$, (f) $\epsilon = 1.3$, (g) $\epsilon = 2.0$, (h) $\epsilon = 3.0$, (i) $\epsilon = 4.0$, (j) $\epsilon = 5.0$, (k) $\epsilon = 10.0$.

a dynamic field a network of resonance zones is induced in the system. The specific form this network takes is determined by the spectrum of the unperturbed system. These resonance zones introduce large fluctuations in the energy of the oscillator. As we have seen, the external field also introduces chaos in the Toda lattice in the sense that the energy of the lattice begins to wander in an apparently random manner and the spectrum becomes broadened. For low-amplitude fields, the theory we have developed gives a good qualitative idea of the behavior of the phase space.

The spectrum of the Toda potential consists of equally spaced lines, whereas the spectra of potentials such as the Lennard-Jones or Morse potentials become more closely spaced at higher frequencies. Thus, the Lennard-Jones and Morse potentials should be more susceptible to the induction of chaos in an external field than is the Toda potential.

ACKNOWLEDGMENTS

The authors wish to thank Thomas Mayer for many helpful discussions. Two of us (L.E.R. and R.d.F.) wish to thank the U.S. Air Force for partial support of this work through Contract No. F33615-78-D-0617. Some of us (R.d.F, T.P., and W.M.Z.) also wish to thank the Welch Foundation of Texas for partial support of this work.

[1]E. Fermi, J. R. Pasta, and S. M. Ulam, *E. Fermi: Collected Papers, Vol. II* (University of Chicago Press, Chicago, 1965), p. 978.

[2]M. Henon and C. Heiles, Astron. J. 69, 73 (1964).

[3]A. N. Kolmogorov, in *Foundations of Mechanics,* edited by R. Abraham (Benjamin, New York, 1967), Appendix D.

[4]V. I. Arnol'd, Russ. Math. J. 18, 9 (1963); 18, 85 (1963).

[5]J. Moser, Nachr. Akad. Wiss. Gottingen, Math.-Phys. Kl. 2 1 (1962).

[6]B. V. Chirikov, Phys. Rep. 52, 263 (1979).

[7]C. H. Walker and J. Ford, Phys. Rev. 188, 416 (1969).

[8]M. Toda, J. Phys. Soc. Jpn. 22, 431 (1967); 23, 501 (1967); J. Phys. Soc. Jpn. Suppl. 26, 235 (1969); Prog. Theor. Phys., Suppl. 45, 179 (1970).

[9]H. Flaschka, Phys. Rev. B 9, 1929 (1979).

[10]M. Kac and P. Van Moerbeke, Proc. Natl. Acad. Sci. USA 72, 2879 (1975).

[11]J. Dancz and S. A. Rice, J. Chem. Phys. 67, 1418 (1977).

[12]Wei-Mou Zheng (unpublished).

[13]The expansion technique we have used does not converge for long time because resonance points are densely distributed in phase space. For each transformation we obtain a new Hamiltonian of order ϵ^n which is valid on a time scale $t \sim e^{(n+1)}$ and in a region of phase space which excludes resonance zones obtained by previous transformations. When resonance zones obtained from Hamiltonian of order $\epsilon^{n'}$ overlap with those of order ϵ^n $(n' < n)$ the Hamiltonian of order ϵ^n is no longer meaningful. This implies that the phase space will be strongly distorted in the overlap region. Thus if we truncate the expansion technique at ϵ^n, the resonance overlap condition gives us an upper bound on the value of ϵ at which overlap may occur.